



Underwater capillary rise

Victoria-Elena Plopeanu[✉], Ioana Rasuceanu[✉] and Claudiu Patrascu[✉]

Hydraulics Department, University POLITEHNICA Bucharest, Splaiul Independentei 313, Bucharest 060042, Romania

Corresponding author: Claudiu Patrascu, claudiu.patrascu@upb.ro

(Received 16 January 2025; revised 8 July 2025; accepted 8 July 2025)

Underwater capillary tubes fill rapidly with the surrounding liquid. Capillary and hydrostatic pressures push the liquid into the tube, causing the air to exit as bubbles at the other end. We study the natural filling process of a vertical capillary tube immersed in water during several bubble formation events. A theoretical model is proposed that captures the dynamics of the meniscus inside the capillary tube as it fills with water. We find good agreement with the experimental data that describe this special case of spontaneous flow using a dynamic contact angle model based on molecular kinetic theory.

Key words: capillary flows, contact lines, bubble dynamics

1. Introduction

Capillary rise describes the spontaneous and natural flow of wetting liquids in narrow spaces with characteristic length scales smaller than the capillary length. It is a long-standing fluid flow phenomenon that has gained momentum with emerging fields such as miniaturisation and microfluidics. The ability of the liquid to flow without external intervention is now at the heart of many practical applications, such as capillary pumps and biochip-integrated systems for drug delivery and testing, with recent developments in the capillary rise of liquids in sharp corners (Wu, Duprat & Stone 2024), liquid–liquid displacement in glass capillaries (André & Okumura 2020; Patrascu & Rasuceanu 2022), the flow of shear-thinning fluids (Steinik *et al.* 2024; Wang *et al.* 2024), capillary rise in partially saturated porous media (Siddique & Anderson 2024), peristome-like microstructured capillary tubes that actuate larger amounts of liquid (Li *et al.* 2019; Liu *et al.* 2024), and rough capillary rise (Panter *et al.* 2023).

In a typical capillary rise experiment, a narrow tube is placed in contact with the free surface of a liquid. The liquid will naturally flow into the tube due to the negative capillary pressure supported by the liquid meniscus. To describe the flow dynamics, one tries to predict the position of the meniscus in time as the level of the liquid rises. Flows in submerged capillary tubes represent a distinct subclass of capillary rise phenomena.

Previous studies have shown that superhydrophobic capillary tubes immersed in water are invaded by air, a phenomenon known as capillary descent, which represents an inverted capillary rise problem with distinct dynamical features (Delannoy *et al.* 2018). Mullins & Braddock (2012) have discussed the capillary rise of a liquid within a partially immersed moving tube. The authors developed a model for the capillary rise in tubes continuously immersed into or removed from a liquid reservoir.

Walls, Dequidt & Bird (2016) have studied submerged capillary tubes filled with the surrounding liquid. Their study discusses the capillary flow of a two-liquid system in a vertical, submerged, capillary tube, emphasising how viscosity and gravity modify the dynamics of spontaneous displacement in the early and late viscous regimes.

Immersed capillaries are also at the core of bubble formation processes. Chuang & Goldschmidt (1970) studied the bubble formation process from an immersed capillary tube in quiescent and coflowing streams by actively controlling the gas flow rate. Blanchard & Syzdek (1977) have proposed a relation between the size of the bubbles and the capillary tube's inner radius. Oguz & Prosperetti (1993) have shown the existence of different growth regimes determined by a critical value of the gas flow rate, and studied the degree of control on bubble size that can be gained by immersing the capillary in a parallel upward flow. The immersed capillary method has been considered in the study of the bubble formation process at specific pressures, and also to establish the role of surface tension on bubble growth (Vazquez, Leifer & Sánchez 2010, Boubendir, Chikh & Tadrist 2020).

Most previous studies within the research area involving immersed capillary tubes explore the displacement of another immiscible liquid by capillary action or the bubble formation process by controlling the gas flow rate. We have found no reference to the natural filling process of a vertical capillary tube immersed in water. The present study extends the domain of capillary flows to underwater capillaries, with contributions to the development of potential applications in the absorption kinetics of underwater recycled aggregates (Liang *et al.* 2021), submersible capillary sensors and analysers (Drevinskas *et al.* 2023), water-based energy devices and capillary pumps (Huang *et al.* 2016), and underwater capillary adhesion strategies (Zheng *et al.* 2022).

We examine the natural filling process of a submerged, empty, capillary tube in water. We perform experiments describing the spontaneous flow dynamics in underwater capillaries, and present a theoretical model that captures the relevant features of the filling process. The paper is structured as follows. Section 2 describes in detail the natural filling process of a submerged capillary tube, § 3 shows the derivation of the theoretical model, and § 4 presents a comparison between the experimental data and the predictions, also highlighting the limitations of the theoretical model.

2. The natural filling process of a submerged capillary tube

Consider a vertical capillary tube submerged in water, with its lower end in contact with a flat solid material that blocks water from entering the tube before its complete immersion. If we slightly move the capillary tube away from the solid material, then water will invade and eventually fill the entire tube. As water invades the capillary tube, the air exits at the other end and forms a bubble. A typical filling process is shown in figure 1, with a detail of the bubble that forms and detaches at the other end of the capillary.

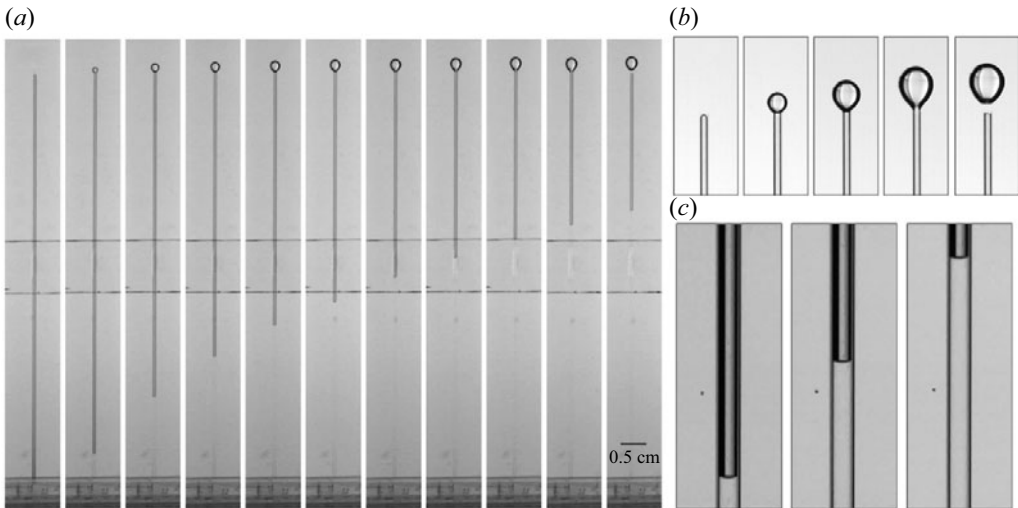


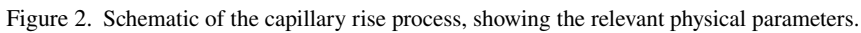
Figure 1. (a) Images showing a submerged capillary tube and its natural filling process, with a bubble forming at the other end (39 ms between each frame). (b) As water enters the capillary, the air is removed as a bubble that detaches from the tube when buoyancy exceeds the surface tension forces. (c) Images showing a typical water–air meniscus that contributes to the filling process of a capillary tube (0.42 mm in diameter).

The filling process is driven by capillarity and the hydrostatic pressure difference between the two ends. The convex liquid meniscus that forms inside the tube (shown in [figure 1c](#)) sustains a capillary pressure that forces the liquid to rise and fill the tube. Depending on the tube's radius and length, the hydrostatic pressure difference can also significantly contribute to the initial stages of the filling process. As water rises in the capillary, the process is resisted by a combination of gravitational, viscous and inertial effects.

The movement of water in capillary tubes has been a long-standing problem since the early works of Bell & Cameron (1906), Lucas (1918) and Washburn (1921), where the derivation of the equation of motion assumes capillary action, a fully developed Poiseuille flow, and a constant contact angle. Later studies by Blake & Haynes (1969), Hoffman (1975), Voinov (1976), Cox (1986) and Bracke, De Voeght & Joos (1989) have emphasised the dynamic nature of the contact angle. The flow depicted in [figure 1](#) is also a function of the dynamic contact angle of the meniscus, a characteristic feature of all capillary rise phenomena. The description of such flows always requires the coupling of the governing equations with a model that considers the velocity dependence of the contact angle.

A distinct feature of underwater capillary rise is the airflow at the outlet. Compared with the classical case of capillary rise where the end tip is practically surrounded by the same fluid that exits the tube, for an immersed capillary tube, the air is removed underwater. The flow expels air from the capillary tube in the form of bubbles at the other end. In the process, the bubble also displaces the liquid in which it grows, adding to the resistive forces that shape the capillary flow. This aspect requires the coupling with a bubble-growth model that gives the phenomenon its distinct dynamical trait.

Depending on the tube's length, several bubbles may detach during the filling process. The bubble's detachment may also significantly change the general flow dynamics due to the high capillary pressures that characterise the pitch-off regime, a detail that will be discussed in § 4.3.



3.1. Momentum balance

When both ends are open, the outer liquid (water) will invade the capillary tube because of the combined forces of hydrostatic pressure and capillarity, forcing the air out of the tube as bubbles. We aim to describe the position of the meniscus $z(t)$ as a function of time. The rate of change of the liquid's momentum as it flows into the capillary tube is given by

where $m_l = \pi R^2 z \rho$ is the mass of the liquid, ρ is the density of water, $m_g = \pi R^2 (L - z) \rho_g$ is the mass of the gas, ρ_g is the gas density, and σ represents viscous stresses discussed in more detail below. The first term on the right-hand side represents the force exerted at the entrance with

where \dot{z} denotes the velocity of the liquid.

The second term on the right-hand side can be obtained by considering the pressure jump at the liquid–gas interface via Laplace pressure,

$$p_1 = p_{gi} - \frac{2\gamma}{R} \cos \theta, \quad (3.3)$$

where p_{gi} is the gas pressure at the interface, γ is the surface tension, and θ is the dynamic (apparent) contact angle.

We neglect the viscous resistance of the gaseous phase, $8\pi\eta_g(L-z)\dot{z}$, knowing that $L-z$ and \dot{z} decrease rapidly. Also, Hultmark, Aristoff & Stone (2011) proposed that the viscous contribution of the gaseous phase should be considered when $\eta_g L/(\eta R) \gg 1$. In our case, for the 80 mm long capillaries with inner diameters 0.42 mm and 1.15 mm, we find that the ratios are approximately 8 and 3, respectively, values that are below the required order of magnitude. The same values for this characteristic ratio have been found in several published studies in capillarity where the viscosity of the gaseous phase is neglected (Quéré *et al.* 1999; Wu *et al.* 2017b; Hamraoui *et al.* 2000; Ruiz-Gutiérrez *et al.* 2022).

As the liquid rises into the capillary tube, a bubble forms and grows at the other end. We denote by p_g the air pressure in the bubble. Assuming negligible viscosity for the gas, we write the unsteady Bernoulli equation on a streamline between the interface and the bubble's centre for an inviscid fluid, and obtain $p_{gi} + \rho_g \dot{z}^2/2 = p_g + \rho_g g(L-z+R_b) + \int_A^B \rho_g (\partial v/\partial t) dl$, where the last term can be approximated as $\rho_g \ddot{z}(L-z+R_b)$, with R_b the bubble radius.

We aim to derive an equation for the acceleration of the interface \ddot{z} , and numerically solve in Matlab the resulting differential equation. The procedure requires us to divide all terms by $\pi R^2 \rho z$. Since $\rho_g/\rho \sim 10^{-3}$, and knowing that the velocity of the liquid decreases in time as water enters the capillary tube, we can discard all terms dependent on ρ_g , therefore $p_{gi} \approx p_g$. It is important to mention that one can also opt for keeping all terms dependent on ρ_g in the final equation, but the predictions will not differ substantially (an aspect that has been verified) since the density ratio is three orders smaller than unity.

As the liquid enters the capillary tube, the air exits at the other end of the tube and forms a bubble. We consider the growth of a spherical bubble in a surrounding Newtonian liquid. The bubble's surface moves with velocity \dot{R}_b , displacing the surrounding liquid (Elshereef, Vlachopoulos & Elkamel 2010). Except in extreme conditions, gas viscosity, gas inertia and compressibility effects can be safely neglected (Scriven 1995). The pressure difference at the bubble's surface is then given by

$$p_g - p_e = 4\eta \frac{\dot{R}_b}{R_b} + \frac{2\gamma}{R_b} + \rho \left(R_b \ddot{R}_b + \frac{3}{2} \dot{R}_b^2 \right), \quad (3.4)$$

where η is the viscosity of the liquid, $p_e = p_{at} + \rho g(h_0 - R_b)$ is the hydrostatic pressure far away from the bubble, and R_b is the bubble radius. The equation is also known as the extended Rayleigh equation (Plesset 1949; Scriven 1995). The terms on the right-hand side represent viscous stresses, capillary pressure and liquid inertia. By considering mass conservation, one can relate the position of the liquid in the tube $z(t)$ with the bubble radius $R_b(t)$. We find that the time variation of the bubble's volume is equal to the flow rate of air that enters the bubble,

$$\frac{dV_b}{dt} = \dot{z} \pi R^2 \rightarrow 4\pi R_b^2 \frac{dR_b}{dt} = \frac{dz}{dt} \pi R^2 \rightarrow \int_0^{R_b} 4\pi R_b^2 dR_b = \int_{z_0}^z \pi R^2 dz, \quad (3.5)$$

which yields

$$R_b = \frac{1}{2}(6R^2)^{1/3}(z - z_0)^{1/3}, \quad (3.6)$$

where we have considered the general case when initially the tube is filled up to z_0 with water. This would correspond to cases when multiple bubbles form and detach during the filling process of the capillary tube. For an empty capillary tube, $z_0 = 0$. Combining (3.6) and (3.4), we obtain

$$p_g = p_e + \frac{4\eta\dot{z}}{3(z - z_0)} + \frac{4\gamma}{(6R^2)^{1/3}(z - z_0)^{1/3}} + \frac{\rho(6R^2)^{2/3}\ddot{z}}{12(z - z_0)^{1/3}} - \frac{\rho(6R^2)^{2/3}\dot{z}^2}{72(z - z_0)^{4/3}}. \quad (3.7)$$

The third term on the right-hand side of (3.1) represents viscous friction, where $\sigma = -4\eta\dot{z}/R$ are the viscous stresses assuming a local Poiseuille flow, and the fourth term represents the weight of the liquid column.

After replacing p_0 , p_1 and σ , we divide (3.1) by $\rho\pi R^2z$ and obtain the acceleration

$$\ddot{z} = \left[\frac{gL}{z} - \frac{3\dot{z}^2}{2z} - \frac{8\eta\dot{z}}{\rho R^2} - g + \frac{2\gamma}{\rho R z} \cos \theta + \frac{g(6R^2)^{1/3}(z - z_0)^{1/3}}{2z} - \frac{4\eta\dot{z}}{3\rho z(z - z_0)} - \frac{4\gamma(z - z_0)^{-1/3}}{\rho z(6R^2)^{1/3}} + \frac{(6R^2)^{2/3}\dot{z}^2}{72z(z - z_0)^{4/3}} \right] / \left(1 + \frac{(6R^2)^{2/3}}{12z(z - z_0)^{1/3}} \right). \quad (3.8)$$

3.2. Dynamic contact angle model

The dynamic contact angle θ is considered via the molecular-kinetic theory (Blake 2006; Wu *et al.* 2017b), which considers the adsorption and desorption dynamics of liquid molecules on a solid surface near the three-phase contact line. The velocity-dependent contact angle can be written in the form

$$\cos \theta = \cos \theta_e - \zeta \frac{\eta\dot{z}}{\gamma}, \quad (3.9)$$

where θ_e is the equilibrium contact angle, and

$$\zeta = \frac{\mathcal{V}_m}{\lambda^3} \exp \left[\frac{\lambda^2 \gamma (1 + \cos \theta_e)}{k_B T} \right], \quad (3.10)$$

where \mathcal{V}_m is the molecular volume, λ is the distance between the adsorption sites on a solid surface, $\gamma(1 + \cos \theta_e)$ is the work of adhesion, k_B is the Boltzmann constant, and T is the absolute temperature (Wu *et al.* 2017b).

We numerically solve (3.8) and (3.9) in Matlab, with ζ as a fitting parameter for one set of experimental data (the capillary rise of water in a tube of 0.42 mm diameter during the first bubble formation process), then use it to predict the position of the liquid–air interface inside another capillary tube with a larger diameter during multiple bubble formation processes. We then compute λ using (3.10), and find it to be extremely close to previously reported values (Wu *et al.* 2017b). Experimental data and comparisons with predictions are given below.

4. Experiments

4.1. Experimental details

The experiment requires the immersion of a glass capillary tube in water. First, we vertically position a capillary tube in an empty container, then we gently put the lower end in contact with a flexible, flat, silicone material (PDMS) to prevent water from entering the tube during the filling process of the container. When the water level exceeds the upper end of the capillary tube, we gently lift the capillary and let water naturally enter the tube.

We used soda-lime glass capillary tubes with inner diameters 0.42 and 1.15 mm, both 80 mm long. The working liquid is water with $\rho = 998 \text{ kg m}^{-3}$, $\eta = 0.85 \text{ mPa s}$, $\gamma = 71.7 \text{ mN m}^{-1}$, and capillary length $l_c = (\gamma/\rho g)^{0.5} = 2.7 \text{ mm}$ at 27°C . The position of the meniscus in the capillary tube during the filling process was recorded using a high-speed camera (Photron FASTCAM UX 100) working at 4000 fps.

The equilibrium contact angle θ_e was determined by placing the glass capillary tubes in contact with water. By measuring the equilibrium height H_{eq} in several capillary tubes, and using Jurin's law $H_{eq} = 2\gamma \cos \theta_e / (\rho g R)$, we obtain the equilibrium contact angles for glass capillary tubes that are (i) 0.42 mm in diameter, $\theta_e = 42.5 \pm 0.3^\circ$, and (ii) 1.15 mm in diameter, $\theta_e = 25.5 \pm 5.6^\circ$. We considered that equilibrium was reached after waiting 160 min from the contact with the liquid bath, after which we observed no capillary rise. This procedure for determining the equilibrium contact angle corresponds to previously published papers that have reported greater equilibrium heights due to pinning forces attributed to the imperfections of real surfaces (Schäffer & Wong 2000; Zhao *et al.* 2023).

The fitting parameter ζ , needed to compute the velocity-dependent contact angle, was obtained by generating trial numerical solutions of (3.8) and (3.9). We use an error function similar to that defined by Ruiz-Gutiérrez *et al.* (2022). For each trial, we compute

$$\epsilon = \frac{1}{N} \sum_{i=1}^N |z_i^{exp}(t_i) - z(t_i)|, \quad (4.1)$$

where N is the number of data points, $z_i^{exp}(t_i)$ is the position of the interface inside the capillary tube at time t_i , and $z(t_i)$ is the corresponding prediction. We search for the minimum of ϵ by incremental variation of ζ , then numerically solve (3.10) for λ in the range of nanometres. The fitting is done for the capillary rise of water in a tube of diameter 0.42 mm during the first bubble formation process. The value was then used to predict the position of the liquid–air interface inside the capillary tube with a larger diameter during multiple bubble formation processes. The values of the error function ϵ were found to be lower than 0.55 mm.

4.2. Experimental data and model predictions

The experiments target the filling process of a capillary tube submerged in water. Figure 3(a) shows two sets of repeated experiments and corresponding data for the meniscus position as a function of time for two capillary tubes with different diameters. As water rises in the capillary tube, the air exits at the other end as a bubble. Buoyancy increases as the air accumulates into the bubble, initiating the detachment process. For the smaller capillary tube ($D = 0.42 \text{ mm}$), the first bubble detaches after the liquid moves more than 50 mm from the lower end. The bubble's detachment process induces significant changes to the dynamics of the advancing water column due to higher capillary pressures created by the necking process. The capillary tube's length (80 mm) does not allow the formation of multiple successive bubbles since over 50 mm is needed for the natural

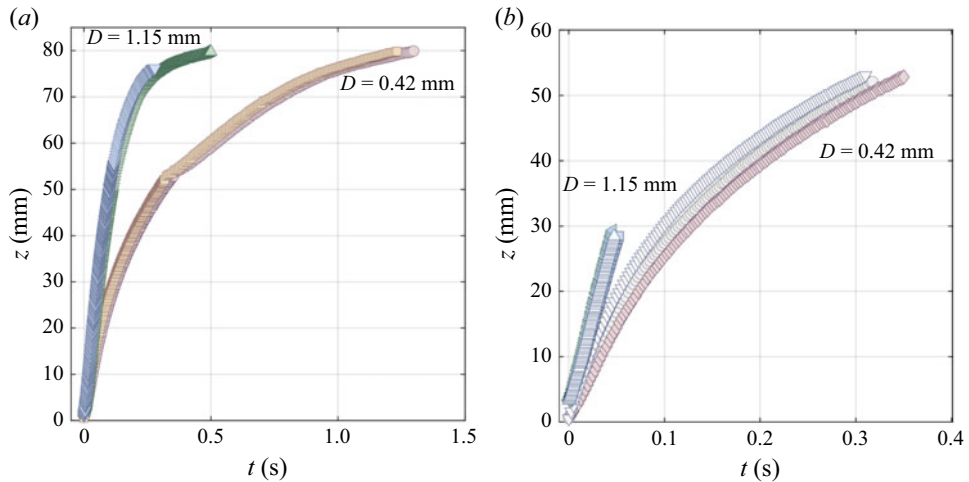


Figure 3. (a) Experimental data of the position z as a function of time for several capillary filling processes. The data represent two experiments for two capillary tubes with different inner diameters. (b) Three sets of experimental data showing the meniscus position in time until the first bubble detaches from the other end of the capillary tube.

detachment process. The last bubble can detach or remain pinned at the upper end of the capillary tube, depending on the glass surface roughness and the contact line that forms during the bubble formation process.

The larger capillary tube ($D = 1.15$ mm) gives three complete, consecutive bubbles during the filling process. Each detachment process has less impact on the overall dynamics due to lower capillary pressures during the necking of the bubble, and higher inertia due to larger masses of liquid contained by the tube. The last bubble (the fourth) may not detach from the capillary due to contact line pinning. Also, we observed that the contact line settles inside the capillary tube at approximately one millimetre below its tip.

The model described by (3.8) and (3.9) was used to describe the observed dynamics of the capillary rise of water for an immersed capillary tube. Figure 3(b) shows three sets of experimental data depicting the position of the liquid meniscus inside the capillary tube during the formation of the first bubble. The figure shows data for both capillary tubes (0.42 and 1.15 mm in diameter). The data were used to compute the average value of z at each instant in time, and the corresponding standard deviation.

To test the model, we fit the prediction by varying ζ until we obtain the minimum value of the error function ϵ . The fit was done on one set of experimental data for the capillary rise in a tube of 0.42 mm diameter during the formation process of the first bubble (initial conditions $z_0 = z(0) = 0$ and $\dot{z}(0) = 0$). We find $\zeta = 105$ with error $\epsilon = 0.55$ mm.

Figure 4(a) shows the model's predictions compared to experimental data representing a typical filling process. We observe that a constant contact angle approach overestimates the data, emphasising the importance of the variation of the contact angle with respect to velocity. In figure 4(b), we also plot the model's prediction considering a static contact angle model ($D = 0.42$ mm, $\zeta = 0$). We incrementally vary the equilibrium contact angle from the measured value 42.5° to 72.5° . The predictions show large deviations compared to the measured values of the liquid's position in the capillary tube. Even if in some cases the prediction seems to gradually enter the margin of error, the overall trend does not capture the proper dynamics of the system (which is well captured only by the dynamic contact angle model – the continuous black curve).

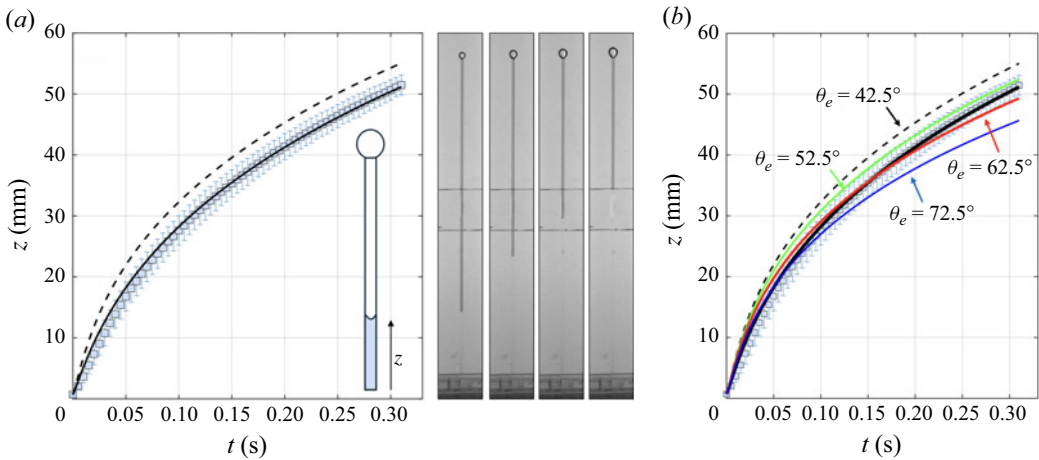


Figure 4. (a) Model predictions (dashed line indicates constant contact angle, solid line indicates dynamic contact angle) and experimental data for the capillary rise of water in a completely submerged tube of 0.42 mm diameter during the formation of the first bubble. The relevant parameters are given in table 1. The images on the right show a typical filling process. (b) Sensitivity of the predictions to a change in the equilibrium contact angle when a static contact angle model is assumed.

The analysis shows that the model needs to include a dissipation that occurs at the moving contact line. The motion induces a deformation of the meniscus, which is only captured by the dynamic contact angle models. Without taking into account the dynamic nature of the contact angle, one cannot capture the proper capillary rise dynamics as shown by the data and also represent the actual physical picture of the moving contact line, which shows a variation in the contact angle.

We emphasise that the standard deviation of the experimental data is below one capillary length, and the model offers a good prediction for the underwater capillary rise problem when $\zeta = 105$.

Using the definition of ζ in the molecular-kinetic theory, here shown by (3.10), we can calculate the value of λ , the distance between adsorption and desorption sites. Knowing that $\mathcal{V}_m = 2.989 \times 10^{-29} \text{ m}^3$, $\gamma = 71.7 \text{ mN m}^{-1}$, $\theta_e = 42.5^\circ$, $k_B = 1.38064 \times 10^{-23} \text{ J K}^{-1}$ and $T = 300.15 \text{ K}$, we find $\lambda = 0.43 \text{ nm}$, which is extremely close to previously reported values (0.44–0.56 nm) in studies involving the capillary rise of several other liquids (Wu *et al.* 2017b).

The model was then used to predict the filling process of a larger capillary tube ($D = 1.15 \text{ mm}$) during which several complete bubble formation processes occur. Table 1 gives all the relevant parameters to compute the predictions. The initial velocity of the water column for the second, third and fourth bubbles is determined by the linear fit of the last five data points (t_i, z_i) measured before the new bubble formation process begins. Also, for each new bubble formation process, we reset the time to zero, and aim to predict the position of the liquid inside the capillary tube as a function of time using (3.8) and (3.9).

Figure 5 shows the position of the liquid as a function of time, and the corresponding prediction (continuous line) during the filling process of a capillary tube of 1.15 mm diameter. The predictions agree well with the data, the error functions being lower than 0.36 mm (as shown in table 1) with $\zeta = 105$ as obtained earlier. We emphasise that the predictions were not obtained in this case via fitting, the approach aiming at testing the model's predictive power. The parameter ζ was calculated by fitting the experimental data obtained in the experiments where we used the capillary tube with a smaller diameter (0.42 mm).

Capillary diameter (mm)	θ_e (deg.)	Bubble index	L (mm)	z_0 (mm)	$\dot{z}(0)$ (m s ⁻¹)	ζ	ϵ (mm)
0.42	42.5	1	80	0	0	105	0.55
		2	80	52.7	0.08	105	–
1.15	25.5	1	80	3.2	0	105	0.20
		2	80	28.8	0.543	105	0.11
		3	80	53	0.297	105	0.36
		4	80	69	0.128	105	–

Table 1. The set of parameters for the model predictions. The parameters are given for each successive bubble formation process. The liquid is water at 27 °C, with $\eta = 0.85$ mPa s, $\rho = 998$ kg m⁻³ and $\gamma = 71.7$ mN m⁻¹.

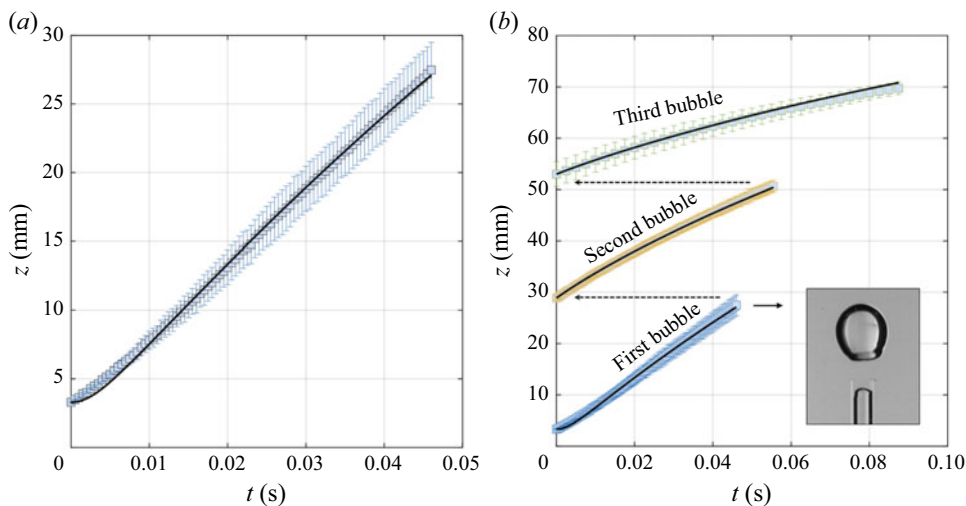


Figure 5. Model predictions (continuous line) and experimental data for the capillary rise of water in a tube of 1.15 mm diameter during the formation of (a) the first bubble, and (b) three consecutive bubbles. The parameters for the predictions are given in table 1.

Conversely, we can also use the model to fit the data from figure 5 and determine λ , using ζ as the fitting parameter, ensuring a minimum for the error function, for each of the three capillary rise processes that correspond to the three consecutive bubbles. Using this approach, we find that the average value is $\lambda = 0.417 \pm 0.013$ nm. The analysis shows that λ is approximately the same for all experiments conducted in the same type of glass capillaries.

We also tested the model's predictions under the assumption that the dynamic contact angle is described by the hydrodynamic model (Cox 1986), $\theta^3 = \theta_e^3 + 9\chi\eta\dot{z}/\gamma$. The predictions overlap with the molecular-kinetic theory model when $\chi = 38$, as shown in figure 6. In the literature, the parameter ranges from 8 to 30 for several other tested liquids (Katoh *et al.* 2015; Wu *et al.* 2017b). For the range of capillary numbers that correspond to the filling process ($Ca = \eta\dot{z}(t)/\gamma < 0.0057$), both models predict approximately the same variation for the contact angle. Another model for the dynamic contact angle is the self-layering model, $\cos \theta = \cos \theta_e - \beta\eta\dot{z}/\gamma$, with $\beta = \exp[2\gamma/W(0)]$, and $W(0)$ as the entropic solvation energy extrapolated to zero distance from the solid surface (Wu *et al.* 2017a,b). Compared with the model given by (3.9), the model is equivalent (only in written form) to the molecular-kinetic theory model, meaning that we can use the previous fit to

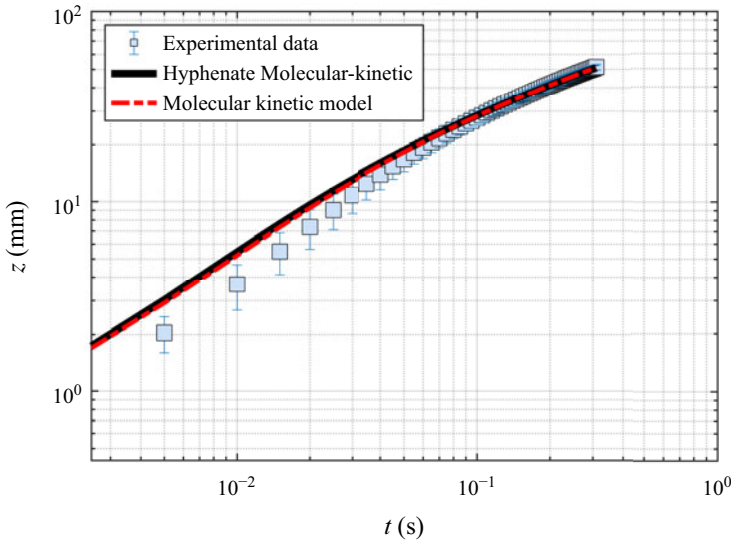


Figure 6. Model predictions for a dynamic contact angle described by the hydrodynamic model versus molecular-kinetic theory compared to experimental data. The data are given for the capillary rise of water in a tube of diameter 0.42 mm.

determine β . Writing $\beta = \zeta = 105$, this gives $W(0) = 2\gamma / \ln(105) \approx 30.8 \text{ mN m}^{-1}$ for the entropic solvation energy extrapolated to zero distance from the solid surface. Considering that the dynamics of the contact angle is not fully understood, the interpretation of the numerical values of both parameters is still a matter of scientific debate, especially when considering the role of inertia in the description of the contact line flow for fluids with low viscosity (Bonn *et al.* 2009) or the local temperature change in the vicinity of the dynamic contact line (Kusudo *et al.* 2023).

4.3. Limitations and interpretations of the model

The model can describe the filling process only until the bubble detaches at the other end. We can approximate beforehand the height of the water column inside the capillary tube that will result in the formation and detachment of a bubble if we assume that detachment occurs when the buoyancy force is approximately equal to the surface tension force, $\rho g \mathcal{V} \sim \pi D \gamma$. The air that forms the bubble is displaced by the advancing water column of length z_c , which implies $\mathcal{V} = z_c \pi D^2 / 4$. We obtain $z_c = 4l_c^2 / D$, where l_c is the capillary length. In the last equation, we emphasise an interesting aspect: the resemblance to Jurin's law for the equilibrium height in the case of a liquid that completely wets the tube. Tubes with a length greater than $4l_c^2 / D$ will generate two or more bubbles. Since, in practice, it is difficult to manufacture capillary tubes of a specific length, one is forced to use standard lengths provided by the manufacturer. In our study, the capillary tubes are 80 mm long, giving two bubbles when $D = 0.42 \text{ mm}$, and four bubbles when $D = 1.15 \text{ mm}$. To avoid bubble detachment, one would need capillaries smaller than $4l_c^2 / D$. Even if the option of manufacturing capillary tubes of a specific length were commercially available, the detachment of the bubble does not take place exactly when the liquid reaches the calculated critical height because the detachment process of the bubble is dependent on the irregularities of the capillary tube's tip, which are an artefact of the manufacturing process. Even with these limitations, the model can be used to accurately predict the filling process when

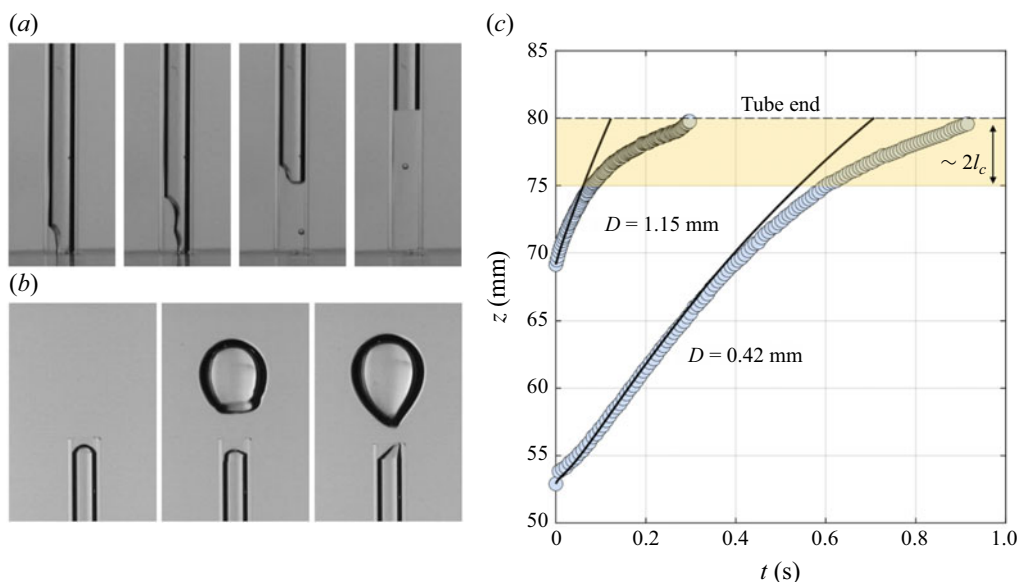


Figure 7. (a) Images showing the water–air interface in the first 24 ms as water invades a capillary tube of 1.15 mm diameter. (b) The water–air interface at the other end of the capillary tube at the beginning of the filling process (the image on the left) and after bubble detachment. (c) The model predictions and experimental data that correspond to the final stage of the filling process for which bubble detachment was observed. The relevant parameters are given in [table 1](#).

multiple bubbles form by changing the model’s initial conditions concerning the position of the interface inside the capillary and the initial velocity (as depicted in [figure 5b](#)).

The prediction fits the data quite well during the first process of bubble formation, even though when water enters the capillary, one observes a highly irregular shape of the water–air interface. The phenomenon is more pronounced in capillary tubes with larger diameters, as shown in [figure 7\(a\)](#). This is due to the hydrostatic pressure that forces water into the tube. The contact line pins to local surface irregularities and suffers major deviations from the convex meniscus seen in capillary rise. Since this phenomenon adds to the dissipative forces that accompany the early times of the filling process, the model slightly overestimates the data, as depicted in [figure 6](#). Although the interface starts with a highly irregular shape, it rapidly takes the shape of a convex meniscus that advances into the capillary tube, and the process takes place without major shape alterations until the capillary tube is filled.

It is important to mention that the added mass effect may contribute to the capillary filling process at early times. To incorporate the added mass effect, one has to add $m_a \ddot{z}$ on the left-hand side of (3.1), with $m_a = 7\pi\rho R^3/6$ as the added mass (Ruiz-Gutiérrez *et al.* 2022). Considering the procedure for obtaining the final differential equation, this corresponds to the addition of $7R/(6z)$ in the denominator of (3.8). The term shows that the influence of the added mass decreases rapidly as z increases. We have found that the predictions do not change when considering the added mass term (the corresponding error function remains unchanged at the reported calculated value with two digits after the decimal), which implies that with this particular phenomenon, the effect can be considered as having a minor influence.

Another limitation is related to the bubble detachment process, which induces an adverse pressure that increases due to the capillary pressure exerted by the necking regime

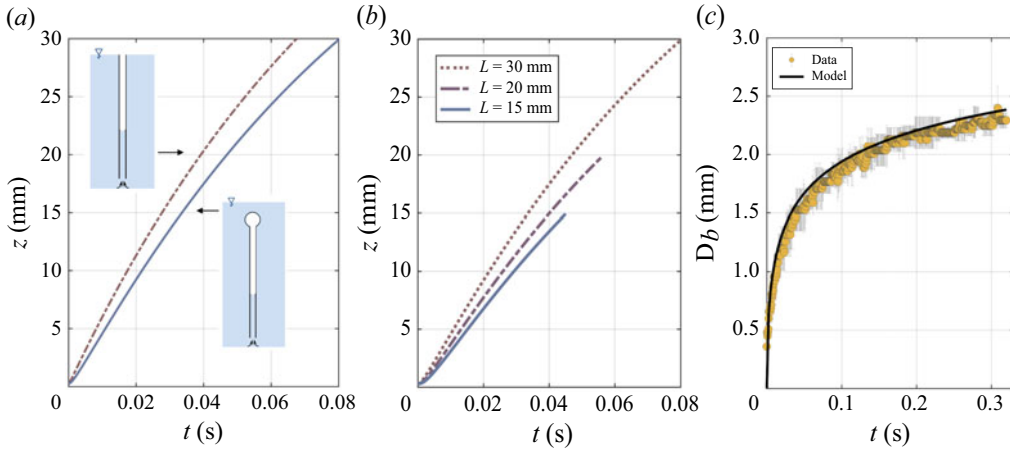


Figure 8. (a) Comparative view of the position of the liquid as a function of time for two immersed capillaries, with one having the end tip in contact with the atmosphere. The predictions are given by (4.2) as a dashed line, and (3.8) as a continuous line. (b) Rise height as a function of time for immersed capillaries of different lengths. The basic configuration for the predictions is given in the text. (c) Model prediction and experimental data for the bubble formation process at the end of a capillary tube with diameter 0.42 mm.

during detachment. Figure 7(b) shows the water–air interface for an empty capillary tube before the filling process starts and after two bubble detachment processes. We observe that the interface settles inside the capillary tube, at approximately 1 mm below the end tip. Furthermore, the last image in figure 7(b) also shows a case of an asymmetric meniscus due to contact line pinning immediately after bubble detachment. The bubble detachment process primarily affects smaller capillary tubes (as clearly visible in figure 3a) because the necking process implies larger capillary pressures. Although bubble break-up affects the capillary rise of the liquid in larger tubes, the effect is not as pronounced as in the latter case.

In figure 7(c), we compare the prediction with the experimental data for the position of the liquid inside the capillary tube, $z(t)$, during the last bubble formation process ending with the bubble's detachment and with it the complete filling of the tube. We also emphasise that the last bubble may not detach due to the contact line or bubble pinning at the tip of the capillary, with a small amount of air remaining inside. We observe large deviations, especially when the last 5 mm is to be filled, which corresponds to approximately two capillary lengths. In this final stage, the advancing meniscus merges with the contact line that supports the bubble, their interaction not being described by the model. The model overpredicts the position of the liquid in this region, the data showing possible extra resistive forces occurring in the last stage of the capillary filling.

One also needs to highlight that the molecular-kinetic approach of the contact line dynamics, which has been incorporated into the present model, has intrinsic limitations that have been highlighted and discussed by Sedev (2015).

The model can also be used to quantify the influence of various characteristic features. To show this, we start with a basic configuration of parameters (for simplicity, $D = 1$ mm, $L = 30$ mm, $\theta = 0$, $\zeta = 0$, $z_0 = 0$, $z(0) = 10\% l_c$, $\dot{z}(0) = 0$, $\eta = 0.85$ mPa s, $\rho = 998$ kg m⁻³, $\gamma = 71.7$ mN m⁻¹), and consider a comparison with the flow in a submerged capillary tube having one end at the free surface. In this situation, no bubble would form

at the tip, the air flowing directly into the atmosphere. Considering the basic configuration given above, the capillary flow is described by the differential equation

$$\ddot{z} = \frac{gL}{z} - \frac{3\dot{z}^2}{2z} - \frac{8\eta\dot{z}}{\rho R^2} - g + \frac{2\gamma}{\rho Rz}, \quad (4.2)$$

which represents the limiting case of (3.8) when the end of the capillary tube is in contact with the atmosphere. Figure 8(a) shows that in the absence of the bubble, the filling process is faster. As expected, the combined resistive forces associated with bubble growth, introduced via capillary pressure, viscous stresses and inertia, considerably delay the filling process, with longer tubes favouring the observed delay. Compared to flows solely driven by the capillary pressure, the flow in immersed tubes is also driven by the hydrostatic pressure difference between the two ends. In figure 8(b), we compare the flow dynamics of three capillary tubes with different lengths, where we observe that the hydrostatic pressure difference increases the velocity of liquid intake. For example, considering the rise height of 10 mm, longer tubes, which correspond to greater hydrostatic pressure differences $\sim \rho g L$, favour the increase of liquid uptake.

One can also plot the time variation of the gas bubble's diameter as the liquid fills the capillary tube using (3.6), which yields $D_b = (6R^2)^{1/3}(z - z_0)^{1/3}$. We measure the time variation of the bubble's diameter, and compare it to the model's predictions for a capillary tube with diameter 0.42 mm, as depicted in figure 8(c). We obtained good quantitative agreement despite the fact that close to detachment, the bubble deviates from the assumed spherical shape, the effect being more pronounced when using larger capillaries.

5. Conclusions

The study shows how underwater capillary tubes naturally fill with the surrounding liquid. As the fluid flows into the tube, the air is removed as bubbles at the other end. The physical description of the flow in an underwater capillary tube includes the coupling of distinct, yet interconnected phenomena, such as capillary rise, contact line dynamics and bubble growth. When these phenomena are coupled, the resulting model provides a good approximation for the filling process of the submerged capillary tube, as shown by comparison with the experimental data.

We present experimental data concerning the capillary rise of water in a submerged empty capillary tube, and derive a theoretical model that also takes into consideration the bubble formation process that takes place at the other of the capillary. The proposed theoretical model captures the advance of the water column as it slows down during the filling process. The last stages of the capillary rise, which also include the merging of the two contact lines, prove to be more difficult to predict with the same accuracy as the earlier filling stages. However, this final regime covers only approximately 7 % of the total rise height, spanning approximately two capillary lengths.

These spontaneous flows provide a fruitful ground for future development, with implications in fundamental and applied sciences. The study can also be extended to describe the natural displacement process of another immiscible liquid that initially occupies the submerged capillary tube for which the flow will now generate a droplet at the other end, a situation that is less encountered in Nature but of great importance in engineering.

Funding. This work was supported by a grant of the Ministry of Research, Innovation and Digitization, CNCS-UEFISCDI, project number PN-IV-P2-2.1-TE-2023-0288, within PNCDI IV.

Declaration of interests. The authors report no conflict of interest.

Data availability statement. The data that support the findings of this study are available upon reasonable request from the corresponding author.

Author contributions. C.P. devised the research, secured funding and developed the theoretical model. C.P., V.-E.P. and I.R. designed and carried out the experiments. V.-E.P. and I.R. ensured data acquisition and analysis. C.P. wrote the manuscript with input from all authors.

REFERENCES

- ANDRÉ, J. & OKUMURA, K. 2020 Capillary replacement in a tube prefilled with a viscous fluid. *Langmuir* **36** (37), 10952–10959.
- BELL, J.M. & CAMERON, F.K. 1906 The flow of liquids through capillary spaces. *J. Phys. Chem.* **10** (8), 658–674.
- BLAKE, T.D. 2006 The physics of moving wetting lines. *J. Colloid Interface Sci.* **299** (1), 1–13.
- BLAKE, T.D. & HAYNES, J.M. 1969 Kinetics of liquid/liquid displacement. *J. Colloid Interface Sci.* **30** (3), 421–423.
- BLANCHARD, D.C. & SYZDEK, L.D. 1977 Production of air bubbles of a specified size. *Chem. Engng Sci.* **32** (9), 1109–1112.
- BONN, D., EGGERS, J., INDEKEU, J., MEUNIER, J. & ROLLEY, E. 2009 Wetting and spreading. *Rev. Mod. Phys.* **81** (2), 739–805.
- BOUBENDIR, L., CHIKH, S. & TADRIST, L. 2020 On the surface tension role in bubble growth and detachment in a micro-tube. *Intl J. Multiphase Flow* **124**, 103196.
- BRACKE, M., DE VOEGHT, F. & JOOS, P. 1989 The kinetics of wetting: the dynamic contact angle. In *Trends Colloid Interface Science III. Progress in Colloid & Polymer Science* (ed. P. Bothorel & E.J. Dufourc), vol. 79. Steinkopff.
- CHUANG, S.C. & GOLDSCHMIDT, V.W. 1970 Bubble formation due to a submerged capillary tube in quiescent and coflowing streams. *J. Basic Engng* **92** (4), 705–711.
- COX, R.G. 1986 The dynamics of the spreading of liquids on a solid surface. Part 1. Viscous flow. *J. Fluid Mech.* **168**, 169–194.
- DELANNOY, J., DE MALEPRADE, H., CLANET, C. & QUÉRÉ, D. 2018 Capillary descent. *Soft Matt.* **14** (26), 5364–5368.
- DREVINSKAS, T., MORA, M.F., SANTOS, F., MAURO, S., NOELL, A.C. & WILLIS, P.A. 2023 Submersible capillary electrophoresis analyzer: a proof-of-concept demonstration of an in situ instrument for future missions to ocean worlds. *Anal. Chem.* **95** (27), 10249–10256.
- ELSHEREEF, R., VLACHOPOULOS, J. & ELKAMEL, A. 2010 Comparison and analysis of bubble growth and foam formation models. *Engng Comput.* **27** (3), 387–408.
- HAMRAOUI, A., THURESSON, K., NYLANDER, T. & YAMINSKY, V. 2000 Can a dynamic contact angle be understood in terms of a friction coefficient? *J. Colloid Interface Sci.* **226** (2), 199–204.
- HOFFMAN, R.L. 1975 A study of the advancing interface. I. Interface shape in liquid–gas systems. *J. Colloid Interface Sci.* **50** (2), 228–241.
- HUANG, S. *et al.* 2016 Underwater spontaneous pumpless transportation of nonpolar organic liquids on extreme wettability patterns. *ACS Appl. Mater. Interfaces* **8** (5), 2942–2949.
- HULTMARK, M., ARISTOFF, J.M. & STONE, H.A. 2011 The influence of the gas phase on liquid imbibition in capillary tubes. *J. Fluid Mech.* **678**, 600–606.
- KATOH, K., WAKIMOTO, T., YAMAMOTO, Y. & ITO, T. 2015 Dynamic wetting behavior of a triple-phase contact line in several experimental systems. *Exptl Therm. Fluid Sci.* **60**, 354–360.
- KUSUDO, H., OMORI, T., JOLY, L. & YAMAGUCHI, Y. 2023 The receding contact line cools down during dynamic wetting. *J. Chem. Phys.* **159** (16), 161102.
- LI, C., DAI, H., GAO, C., WANG, T., DONG, Z. & JIANG, L. 2019 Bioinspired inner microstructured tube controlled capillary rise. *Proc. Natl Acad. Sci.* **116** (26), 12704–12709.
- LIANG, K., HOU, Y., SUN, J., LI, X., BAI, J., TIAN, W. & LIU, Y. 2021 Theoretical analysis of water absorption kinetics of recycled aggregates immersed in water. *Constr. Build. Mater.* **302**, 124156.
- LIU, X., GAO, M., LI, B., LIU, R., CHONG, Z., GU, Z. & ZHOU, K. 2024 Bioinspired capillary transistors. *Adv. Mater.* **36** (41), 2310797.
- LUCAS, R. 1918 Ueber das zeitgesetz des kapillaren aufstiegs von flüssigkeiten. *Kolloid Z.* **23** (1), 15–22.
- MULLINS, B.J. & BRADDOCK, R.D. 2012 Capillary rise in porous, fibrous media during liquid immersion. *Intl J. Heat Mass Transfer* **55** (21–22), 6222–6230.
- OGUZ, H.N. & PROSPERETTI, A. 1993 Dynamics of bubble growth and detachment from a needle. *J. Fluid Mech.* **257**, 111–145.

- PANTER, J.R., KONICEK, A.R., KING, M.A., JUSUFI, A., YEGANEH, M.S. & KUSUMAATMAJA, H. 2023 Rough capillary rise. *Commun. Phys.* **6** (1), 44.
- PATRASCU, C. & RASUCEANU, I. 2022 Capillary flow of water in tubes partially prefilled with oil. *Phys. Rev. Fluids* **7** (11), 114001.
- PLESSET, M.S. 1949 The dynamics of cavitation bubbles. *J. Appl. Mech.* **16**, 277–282.
- QUÉRÉ, D., RAPHAËL, É. & OLLITRAULT, J.-Y. 1999 Rebounds in a capillary tube. *Langmuir* **15** (10), 3679–3682.
- RUIZ-GUTIÉRREZ, É., ARMSTRONG, S., LÉVÊQUE, S., MICHEL, C., PAGONABARRAGA, I., WELLS, G.G., HERNÁNDEZ-MACHADO, A. & LEDESMA-AGUILAR, R. 2022 The long cross-over dynamics of capillary imbibition. *J. Fluid Mech.* **939**, A39.
- SCHÄFFER, E. & WONG, P.Z. 2000 Contact line dynamics near the pinning threshold: a capillary rise and fall experiment. *Phys. Rev. E* **61** (5), 5257.
- SCRIVEN, L.E. 1995 On the dynamics of phase growth. *Chem. Engng Sci.* **50** (24), 3907–3917.
- SEDEV, R. 2015 The molecular-kinetic approach to wetting dynamics: achievements and limitations. *Adv. Colloid Interface Sci.* **222**, 661–669.
- SIDDIQUE, J.I. & ANDERSON, D.M. 2024 Capillary rise in partially saturated rigid porous media. *J. Fluid Mech.* **988**, A36.
- STEINIK, C., PICCHI, D., LAVALLE, G. & POESIO, P. 2024 Capillary imbibition of shear-thinning fluids: from Lucas–Washburn to oscillatory regimes. *Phys. Rev. Fluids* **9** (2), 023305.
- VAZQUEZ, A., LEIFER, I. & SÁNCHEZ, R.M. 2010 Consideration of the dynamic forces during bubble growth in a capillary tube. *Chem. Engng Sci.* **65** (13), 4046–4054.
- VOINOV, O.V. 1976 Hydrodynamics of wetting. *Fluid Dyn.* **11** (5), 714–721.
- WALLS, P.L.L., DEQUIDT, G. & BIRD, J.C. 2016 Capillary displacement of viscous liquids. *Langmuir* **32** (13), 3186–3190.
- WANG, X., YUAN, Z., CHEN, F., YAO, X., YU, F. & WANG, S. 2024, Forced wetting of shear-thinning fluids in confined capillaries. *Langmuir* **40** (40), 21222–21231.
- WASHBURN, E.W. 1921 The dynamics of capillary flow. *Phys. Rev.* **17** (3), 273.
- WU, K., DUPRAT, C. & STONE, H.A. 2024 Capillary rise in sharp corners: not quite universal. *J. Fluid Mech.* **978**, A26.
- WU, P., NIKOLOV, A. & WASAN, D. 2017*a* Capillary dynamics driven by molecular self-layering. *Adv. Colloid Interface Sci.* **243**, 114–120.
- WU, P., NIKOLOV, A.D. & WASAN, D.T. 2017*b* Capillary rise: validity of the dynamic contact angle models. *Langmuir* **33** (32), 7862–7872.
- ZHAO, M., HOSSAIN, A.A., COLOSQUI, C.E. & ROCHÉ, M. 2023 Anomalous near-equilibrium capillary imbibition induced by nanoscale surface topography. *Colloids Surf. A: Physicochem. Engng Aspects* **676**, 132261.
- ZHENG, H. *et al.* 2022 Electrically switched underwater capillary adhesion. *Nat. Commun.* **13** (1), 4584.